A new present-day temperature parameterization for Greenland

Robert S. FAUSTO,[1,2] Andreas P. AHLSTRØM,[1] Dirk VAN AS,[1]
Carl E. BØGGILD,[1,3] Sigfus J. JOHNSEN[2]

[1] *Geological Survey of Denmark and Greenland (GEUS), Øster Voldgade 10, DK-1350 Copenhagen, Denmark*
E-mail: rsf@geus.dk
[2] *Centre for Ice and Climate (CIC), Niels Bohr Institute (NBI), University of Copenhagen, Juliane Maries Vej 32, DK-2100 Copenhagen, Denmark*
[3] *The University Centre in Svalbard (UNIS), Box 156, NO-9171 Longyearbyen, Norway*

ABSTRACT. Near-surface air temperature (2 m) over the Greenland ice sheet (GrIS) is parameterized using data from automatic weather stations located on land and on the ice sheet. The parameterization is expressed in terms of mean annual temperatures and mean July temperatures, both depending linearly on altitude, latitude and longitude. The temperature parameterization is compared to a previous study and is shown to be in better agreement with observations. The temperature parameterization is tested in a positive degree-day model to simulate the present (1996–2006) mean melt area extent of the GrIS. The model accounts for firn warming, rainfall and refreezing of meltwater, with different degree-day factors for ice and snow under warm and cold climate conditions. The simulated melt area extent is found to have reasonable agreement with satellite-derived observations.

INTRODUCTION

Ice sheets respond dynamically to changes in boundary conditions, such as climate variations, basal thermal conditions, and isostatic adjustments of the underlying bedrock. The boundary conditions cause ice sheets to evolve towards a new equilibrium. The response is further influenced by feedback processes which may amplify or mitigate the ice sheet's adjustment to the boundary conditions, or by internal dynamic-flow instabilities that may cause rapid changes in ice volume (Paterson, 1994; Rignot and Kanagaratnam, 2006).

The near-surface air temperature is one of the boundary conditions and is considered to be a relatively straightforward meteorological variable to extrapolate or interpolate on climatic timescales. Temperature fields are, in general, continuous, and horizontal temperature gradients are typically low for long-term climatology, in which the effects of weather systems and fronts average out (Ohmura, 1987; Grotjahn, 1993). Vertical temperature gradients are much larger, and the common practice when extrapolating temperature fields to higher or lower elevations is to assume a constant atmospheric lapse rate (Ohmura, 1987; Reeh, 1991; Ritz and others, 1997). The choice is based on the average observed lapse rate in the free atmosphere and represents a typical moist adiabatic cooling rate. Despite their broad application, it is not clear that free-air lapse rates offer an appropriate estimate of slope lapse rates, which is the difference between near-surface air temperature at two locations divided by the difference in elevation (Pepin and Losleben, 2002; Marshall and others, 2007).

A measure of air temperature's influence on annual ablation is the sum of positive degree-days (PDDs) (Ohmura, 2001). The number of degree-days is defined as the total number of days when the temperature exceeds 0°C in a year (Braithwaite, 1995). Many studies have used this type of model to calculate melt from mean monthly temperatures, which includes a magnitude for temperature fluctuations, σ_{pdd}, that can account for melt within a month with a negative mean temperature. This σ_{pdd} is the standard deviation of the near-surface air temperature and is mainly determined by the diurnal cycle and weather systems (Lefebre and others, 2002). Values of σ_{pdd} in the literature range from 4.5 to 5.5°C (Reeh, 1991; Ritz and others, 1997; Huybrechts and de Wolde, 1999; Tarasov and Peltier, 1999).

The primary motivation for developing a temperature parameterization is to use it with a PDD model to calculate spatial and temporal variability of the surface mass balance in numerical ice-sheet models without a full coupling between atmosphere and ice sheet, which takes a longer time to integrate numerically. Regional climate models would be more suitable to couple to an ice-sheet model in order to model the behaviour of the climate system on short timescales. Unfortunately, models of this type (Box and others, 2006; Fettweis, 2007) cannot be applied in studies of the evolution of the Greenland ice sheet (GrIS) through ice ages with a sufficiently high spatial and temporal resolution, due to poorly constrained parameters, such as radiative fluxes and wind speed. This makes the combination of a temperature parameterization and a PDD model currently the best option for studies of the long-term evolution of ice sheets.

This study aims to improve the near-surface air-temperature parameterization for Greenland with the use of new observations from climate stations located on land, in the ablation zone and up to the dry snow in the accumulation zone on the ice sheet. The parameterization is tested by comparing melt-area observations from satellite algorithms with the calculated melt area from a PDD model. A comparison with a previous study by Ritz and others (1997) is also carried out, to test whether the new parameterization improves the calculated melt area extent.

METHODS

Temperature parameterization

Observations from the Greenland Climate Network (GC-Net) (Steffen and others, 1996; Steffen and Box, 2001), the Geological Survey of Denmark and Greenland (GEUS)

https://doi.org/10.3189/002214309788608985 Published online by Cambridge University Press

Table 1. Details of automatic weather stations (AWS) placed on the ice sheet

Station	Location	Data period dd/mm/yy	Altitude m a.s.l
Data from GEUS			
Sermilik1	61°01.525′ N, 46°52.270′ W	16/5/01 to 16/5/02	350
Sermilik1.2	61°01.525′ N, 46°52.270′ W	16/4/04 to 25/4/06*	350
Tasiilaq2	65°37.200′ N, 38°53.522′ W	1/4/04 to 29/5/04	300
Nuuk2	64°44.174′ N, 49°29.555′ W	1/6/03 to 1/6/06	900
Cryo	75°14.153′ N, 57°44.837′ W	7/5/04 to 17/8/06	200
ImersuaqA	66°17.838′ N, 49°44.782′ W	16/6/99 to 18/3/01	886
Data from GC-Net (CIRES†)			
Swiss Camp	69°34.050′ N, 49°19.283′ W	1/9/95 to 9/5/06	1169
Craw. Pt.1	69°52.783′ N, 46°59.200′ W	1/9/95 to 4/5/06	2022
NASA-U	73°50.517′ N, 49°29.900′ W	1/9/95 to 26/4/06	2369
Humboldt	78°31.600′ N, 56°49.833′ W	1/9/95 to 28/4/05	1995
Summit	72°34.783′ N, 38°30.300′ W	14/5/96 to 2/5/06	3208
Tunu-N	78°00.983′ N, 33°59.000′ W	17/5/96 to 1/1/05	2052
DYE-2	66°28.800′ N, 46°16.733′ W	25/5/96 to 7/5/06	2165
JAR1	69°29.850′ N, 49°41.267′ W	20/6/96 to 10/5/06	952
Saddle	65°59.967′ N, 44°30.050′ W	20/4/97 to 7/5/06	2456
South Dome	63°08.933′ N, 44°49.033′ W	23/4/96 to 1/1/06	2901
NASA-E	75°00.033′ N, 29°59.833′ W	3/5/97 to 3/5/06	2614
Craw. Pt.2	69°54.800′ N, 46°51.283′ W	11/5/97 to 30/5/01	1990
NGRIP	75°05.983′ N, 42°19.950′ W	9/7/97 to 1/1/05	2950
NASA-SE	66°28.750′ N, 42°29.933′ W	24/4/98 to 26/5/05	2393
KAR	69°41.967′ N, 33°00.350′ W	17/5/99 to 7/6/01	2579
JAR2	69°25.150′ N, 50°03.917′ W	2/6/99 to 7/5/06	542
JAR3	69°23.667′ N, 50°18.600′ W	1/1/01 to 27/5/04	283
Peterm. ELA	80°05.033′ N, 58°04.033′ W	25/5/03 to 28/4/06	965
Data from the K-transect (IMAU‡)			
s5	67°03.084′ N, 48°14.463′ W	27/8/03 to 27/8/07	510
s6	67°04.666′ N, 49°23.338′ W	1/9/03 to 31/8/07	1020
s9	67°05.992′ N, 50°07.322′ W	1/9/03 to 31/8/07	1520

*No data in the winter of 2004/05.
†Cooperative Institute for Research in Environmental Sciences.
‡Institute for Marine and Atmosphereic Research Utrecht.

(Ahlstrøm and others, 2008) and the K-transect (Van de Wal and others, 2005) (Table 1) and the automatic weather stations (AWS) of the Danish Meteorological Institute (DMI) (see www.dmi.dk for further information), are used to determine a new present-day near-surface air-temperature parameterization for the GrIS (Fig. 1). This study uses observations from locations on land, in the ablation zone and in the accumulation zone of the GrIS.

A mean monthly temperature is calculated from hourly observations each month in a given year for each station. Subsequently, the annual mean and the July mean temperatures are calculated for each station using all available mean values for the whole period (1996–2006; Table 2). The observations show that the slope lapse rate exhibits a strong seasonal variation, with a minimum in July. This variation needs to be taken into account in order to produce a realistic temperature field.

Following a study by Ritz and others (1997) the annual mean (T_{ma}) and July mean (T_{mj}) temperatures are parameterized as a function of altitude, z_s, latitude, ϕ, and longitude, λ:

$$T_{ma} = d_{ma} + \gamma_{ma} z_s + c_{ma}\phi + \kappa_{ma}\lambda, \quad (1)$$

$$T_{mj} = d_{mj} + \gamma_{mj} z_s + c_{mj}\phi + \kappa_{mj}\lambda, \quad (2)$$

where γ_{ma} is the annual mean slope lapse rate, γ_{mj} is the July mean slope lapse rate, c_{ma} and c_{mj} are coefficients determining the dependence on latitude, κ_{ma} and κ_{mj} determine the dependence on longitude, and d_{ma} and d_{mj} are constants. The values of the coefficients are given in Table 3. The coefficients were optimized by fitting the two parameterization functions to the observed mean temperature values (Table 2), using the least-squares method. The longitudinal dependence is new compared to the study of Ritz and others (1997) and is introduced in order to include the observation that temperatures are generally slightly colder in East Greenland than West Greenland for similar altitudes and latitudes. Mean monthly slope lapse rates (Table 4) are calculated between stations along seven different transects around Greenland in order to determine the variability of γ_{ma} and γ_{mj} used in the temperature parameterization. The transects are established between low-lying stations located in the ablation zone and stations in the accumulation zone on the GrIS (Fig. 1).

Positive degree-days

The PDD method is based on the statistical relationship between positive air temperatures and the melting of snow or ice (Ohmura, 2001). The percentage of days with melt, calculated on a monthly basis, is assumed to be equal to the

https://doi.org/10.3189/002214309788608985 Published online by Cambridge University Press

Table 2. A comparison between the modelled (mod.) temperature distribution and observed data (obs.) from the stations. T_a is the annual mean temperature and T_j is the mean July temperature. The difference (diff.) is calculated between the modelled and observed data. Acc., Abl. and Land denote stations located in the accumulation zone, in the ablation zone or on land, respectively

	Station	Location	T_a mod.	T_a obs.	diff.	T_j mod.	T_j obs.	diff.
1	Swiss Camp	Abl.	−12.25	−11.15	−1.10	−0.01	0.06	0.07
2	Craw. Pt.1	Acc.	−18.01	−16.85	−1.16	−4.82	−5.18	0.36
3	NASA-U	Acc.	−22.88	−22.56	−0.32	−7.19	−7.13	−0.06
4	Humboldt	Acc.	−23.39	−25.51	2.12	−5.51	−5.89	0.38
5	Summit	Acc.	−28.00	−27.54	−0.46	−12.14	−12.39	0.25
6	Tunu-N	Acc.	−24.92	−26.17	1.25	−6.97	−7.52	0.55
7	DYE-2	Acc.	−16.51	−17.84	1.32	−5.09	−4.01	−1.08
8	JAR1	Abl.	−10.80	−10.10	−0.70	1.19	1.08	0.11
9	Saddle	Acc.	−18.12	−19.41	1.29	−6.69	−6.39	−0.30
10	South Dome	Acc.	−18.86	−19.04	0.18	−8.64	−7.66	−0.98
11	NASA-E	Acc.	−26.57	−27.31	0.74	−9.76	−10.30	0.54
12	Craw. Pt.2	Acc.	−17.84	−17.12	−0.72	−4.66	−4.72	0.06
13	NGRIP	Acc.	−27.93	−27.62	−0.31	−10.93	−10.47	−0.46
14	NASA-SE	Acc.	−18.21	−19.66	1.45	−6.53	−6.94	0.41
15	KAR	Acc.	−22.33	−21.03	−1.30	−8.56	−9.05	0.49
16	JAR2	Abl.	−8.13	−6.95	−1.18	3.45	2.80	0.65
17	JAR3	Abl.	−10.22	−6.31	−3.91	1.65	2.56	−0.91
18	Peterm. ELA	Abl.	−18.21	−17.17	−1.04	−0.08	2.39	−2.47
19	Sermilik1	Abl.	−1.00	−1.10	0.10	5.68	4.72	0.96
20	Tasilaq2	Abl.	−4.58	−4.01	−0.57	4.78	3.74	1.04
21	Nuuk2	Abl.	−6.90	−5.33	−1.57	2.26	2.74	−0.48
22	Imersuaq A	Abl.	−8.08	−9.51	1.43	2.06	2.92	−0.86
23	Cryo	Abl.	−9.52	−6.32	−3.20	4.83	4.29	0.54
24	s5	Abl.	−6.26	−5.40	−0.86	4.00	4.01	−0.01
25	s6	Abl.	−9.51	−9.68	0.17	1.19	0.88	0.31
26	s9	Abl.	−12.72	−12.40	−0.32	−1.58	−0.75	−0.83
27	Station Nord	Land	−15.94	−16.90	0.96	2.47	3.40	−0.93
28	Danmarkshavn	Land	−12.17	−12.30	0.13	3.48	3.70	−0.22
29	Ittoqqortoormiit	Land	−7.69	−7.50	−0.19	4.37	3.30	1.07
30	Tasiilaq	Land	−3.01	−1.70	−1.31	6.09	6.03	0.06
31	Prins Chr. Sund	Land	1.10	0.70	0.40	7.11	4.50	2.61
32	Qaqortoq	Land	1.05	0.60	0.45	7.37	7.20	0.17
33	Narsarsuaq	Land	0.87	0.90	−0.04	7.34	10.30	−2.96
34	Paamiut	Land	0.49	−0.80	1.29	7.46	5.60	1.86
35	Nuuk	Land	−1.32	−1.40	0.08	6.89	6.50	0.39
36	Kangerlussuaq	Land	−3.16	−5.70	2.54	6.55	10.70	−4.15
37	Sisimuit	Land	−2.73	−3.90	1.17	6.93	6.30	0.63
38	Aasiaat	Land	−4.57	−4.90	0.33	6.17	5.70	0.47
39	Ilulissat	Land	−4.76	−5.00	0.24	6.26	7.50	−1.24
40	Upernavik	Land	−7.12	−7.20	0.08	5.85	5.20	−0.65
41	Pituffik	Land	−8.58	−11.10	2.52	6.23	4.50	1.73

Table 3. Coefficients for Equations (1) and (2) and their root-mean-square difference (rmsd) in relation to the observed temperatures

	$d_{ma,j}$ °C	$\gamma_{ma,j}$ °C km^{-1}	$c_{ma,j}$ °C ° N^{-1}	$\kappa_{ma,j}$ °C ° W^{-1}	rmsd
Best annual fit					
This study with κ_{ma}	41.83	−6.309	−0.7189	0.0672	1.31
This study without κ_{ma}	46.01	−6.380	−0.7340	0	1.48
This study without land stations	40.96	−6.988	−0.6901	0.0742	1.29
Ritz and others (1997)	49.13	−7.992	−0.7576	0	2.27
Best July fit					
This study with κ_{mj}	14.70	−5.426	−0.1585	0.0518	1.24
This study without κ_{mj}	17.86	−5.494	−0.1681	0	1.35
This study without land stations	13.46	−5.172	−0.1809	0.1049	0.83
Ritz and others (1997)	30.38	−6.277	−0.3262	0	2.02

https://doi.org/10.3189/002214309788608985 Published online by Cambridge University Press

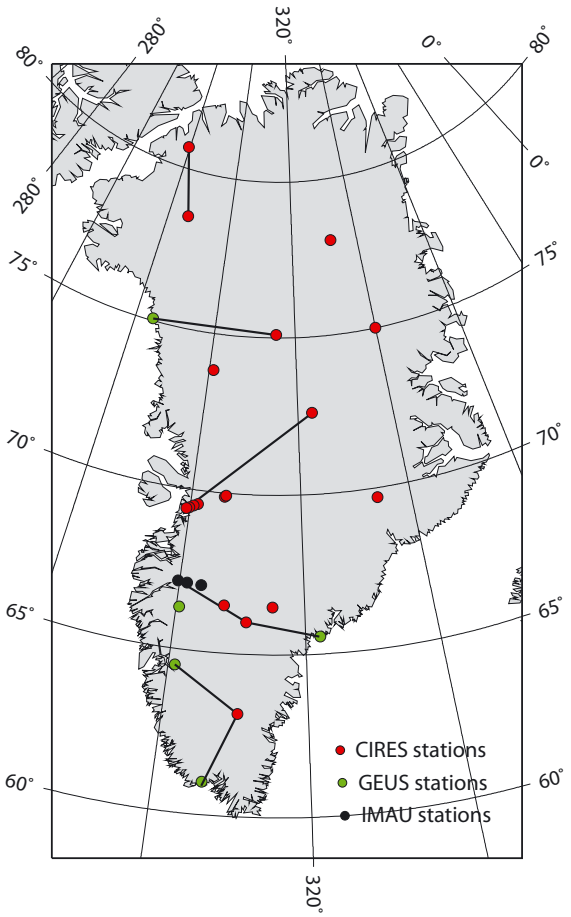

Fig. 1. The locations of the AWS on the ice sheet used in this study. Black lines indicate seven transects used for the slope lapse-rate calculations.

probability that the near-surface air temperature exceeds 0°C and the PDD factors relate the near-surface air temperature to melt of snow or ice (Braithwaite, 1995). Normally, large-scale melt models over Greenland calculate the number of PDDs by assuming an annual sinusoidal evolution of the air temperature (Greve, 2005).

The approach and the values of the degree-day factors are identical to those given by Greve (2005) and are briefly summarized here. The number of PDDs from the normal probability distribution around the monthly mean temperatures during the years is given as:

$$\mathrm{PDD} = \frac{1}{\sigma_{\mathrm{pdd}}\sqrt{2\pi}} \int_0^A \mathrm{d}t \int_0^\infty \mathrm{d}T T \exp\left\{-\frac{[T - T_{\mathrm{a}}(t)]^2}{2\sigma_{\mathrm{pdd}}^2}\right\}, \tag{3}$$

where t is the time, T (°C) is the actual near-surface air temperature and T_{a} (°C) is the annual near-surface temperature cycle. T_{a} is assumed to vary sinusoidally over time,

$$T_{\mathrm{a}}(t) = T_{\mathrm{ma}} + (T_{\mathrm{mj}} - T_{\mathrm{ma}}) \cos\frac{2\pi t}{A}, \tag{4}$$

where A is taken to be 1 year.

Degree-day factors, β_{ice}, β_{snow}, are assumed to be different for ice and snow melt, and for warm ($\beta^{\mathrm{w}}_{\mathrm{ice}}$, $\beta^{\mathrm{w}}_{\mathrm{snow}}$) and cold ($\beta^{\mathrm{c}}_{\mathrm{ice}}$, $\beta^{\mathrm{c}}_{\mathrm{snow}}$) climate conditions. South of 72° N the degree-day factors are assumed to be under warm conditions:

$$\beta_{\mathrm{ice}} = \beta^{\mathrm{w}}_{\mathrm{ice}}, \quad \beta_{\mathrm{snow}} = \beta^{\mathrm{w}}_{\mathrm{snow}}, \tag{5}$$

Table 4. Mean monthly slope lapse rates and their standard deviation from seven transects (see Fig. 1)

Month	Mean monthly slope lapse rate (std dev.) °C km^{-1}
Jan	−7.9 (±4.6)
Feb	−8.9 (±3.5)
Mar	−7.9 (±2.8)
Apr	−7.3 (±2.3)
May	−5.9 (±2.7)
Jun	−4.7 (±0.6)
Jul	−4.6 (±0.6)
Aug	−5.7 (±0.8)
Sep	−6.9 (±2.2)
Oct	−7.3 (±3.1)
Nov	−6.5 (±3.5)
Dec	−7.6 (±3.7)
Mean	−6.8 (±2.5)

where $\beta^{\mathrm{w}}_{\mathrm{ice}} = 7$ and $\beta^{\mathrm{w}}_{\mathrm{snow}} = 3$ mm w.e. d^{-1} °C^{-1}. Cold conditions prevail north of 72° N, and the mean July near-surface air temperature, T_{mj}, is used to calculate the degree-day factors:

$$\beta_{\mathrm{ice}} = \begin{cases} \beta^{\mathrm{w}}_{\mathrm{ice}} & T_{\mathrm{mj}} \geq T_{\mathrm{w}}, \\ \beta^{\mathrm{w}}_{\mathrm{ice}} + \frac{\beta^{\mathrm{c}}_{\mathrm{ice}} - \beta^{\mathrm{w}}_{\mathrm{ice}}}{(T_{\mathrm{w}} - T_{\mathrm{c}})^3} \left(T_{\mathrm{w}} - T_{\mathrm{mj}}\right)^3 & T_{\mathrm{c}} \leq T_{\mathrm{mj}} \leq T_{\mathrm{w}}, \\ \beta^{\mathrm{c}}_{\mathrm{ice}} & T_{\mathrm{mj}} \leq T_{\mathrm{c}}, \end{cases} \tag{6}$$

$$\beta_{\mathrm{snow}} = \begin{cases} \beta^{\mathrm{w}}_{\mathrm{snow}} & T_{\mathrm{mj}} \geq T_{\mathrm{w}}, \\ \beta^{\mathrm{w}}_{\mathrm{snow}} + \frac{\beta^{\mathrm{c}}_{\mathrm{snow}} - \beta^{\mathrm{w}}_{\mathrm{snow}}}{(T_{\mathrm{w}} - T_{\mathrm{c}})} \left(T_{\mathrm{mj}} - T_{\mathrm{c}}\right) & T_{\mathrm{c}} \leq T_{\mathrm{mj}} \leq T_{\mathrm{w}}, \\ \beta^{\mathrm{c}}_{\mathrm{snow}} & T_{\mathrm{mj}} \leq T_{\mathrm{c}}, \end{cases} \tag{7}$$

where $\beta^{\mathrm{c}}_{\mathrm{ice}} = 15$ and $\beta^{\mathrm{c}}_{\mathrm{snow}} = 3$ mm w.e. d^{-1} °C^{-1}. The limiting temperature values, $T_{\mathrm{w}} = 10$°C and $T_{\mathrm{c}} = -1$°C, are used to calculate the limiting degree-day factors, which differentiate according to changes in T_{mj}.

The σ_{pdd} in the degree-day integral (Equation (3)) is different to that provided by Greve (2005). The value used here is smaller ($\sigma_{\mathrm{pdd}} = 2.53$) than the value of 4.5 used by Greve (2005). The value of 2.53 is calculated from the mean value of the standard deviation of the mean monthly temperatures throughout the observation period (1996–2006).

The PDD model, combined with the new temperature parameterization, is used to model the current mean melt area extent of the GrIS. Results are tested against satellite-derived observations, that show the area of melt on the ice sheet (Steffen and others, 2004; Fausto and others, 2007; Fettweis and others, 2007; Wang and others, 2007). Three zones are defined: (1) the dry-snow zone where no melting occurs; (2) the melting-snow zone where melting occurs but all the meltwater is refrozen again as superimposed ice or internal accumulation; and (3) the runoff zone where meltwater is lost from the ice sheet. The melt area extent is then defined as the combined area of the runoff zone and the melting-snow zone. The definition corresponds well with the melt area extent categories of the satellite-derived observations because they use the reflected and emitted radiances to set up threshold values for no melting (dry-snow zone) and for melting of snow and ice (melting-snow zone and runoff zone).

https://doi.org/10.3189/002214309788608985 Published online by Cambridge University Press

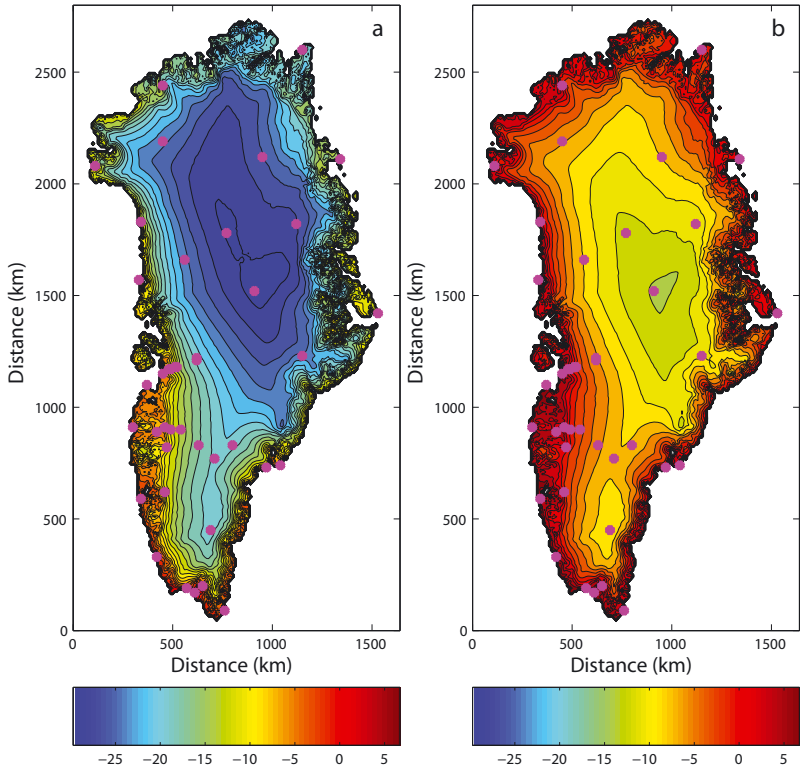

Fig. 2. Parameterized (a) mean annual and (b) mean July temperatures. Dots show the locations of the AWS.

RESULTS

The inclusion of data from the GEUS stations provides a much clearer picture of the slope lapse rates (Table 4). The results from the transects show a great deal of variability, with a distinct seasonal cycle that has a double peak in winter. The largest slope lapse rates are seen in winter and the smallest in summer. The standard deviation of the slope lapse rate is also calculated, with the highest values in the winter and the smallest in the summer (Table 4). The maximum monthly slope lapse rate of $-8.9^{\circ}\mathrm{C\,km^{-1}}$ occurred in February, and the minimum ($-4.6^{\circ}\mathrm{C\,km^{-1}}$) occurred in July. The relatively cold and variable winter temperatures in the interior of the GrIS results in steep slope lapse rates and high standard deviations in contrast to the summer (Table 4). In the summer, the near-surface air temperature can rise further in the interior than at the margin, since temperatures are low enough not to be limited by the ice surface reaching the melting point. The highest standard deviation values of the ablation season (3.0–6.0°C) are found in May, June and September. The lowest values (<2.0°C) occur in July and August.

The optimized values for γ_{ma} in Equations (1) and (2) (Table 3) are well within the standard deviation of the observed values. The discrepancy between γ_{mj} and the observations may be related to the fact that the observed slope lapse rates in Table 4 were calculated without using data from the land stations, while all the available data to determine the coefficients for Equations (1) and (2) were used.

Figure 2 gives a visual presentation of the near-surface air-temperature fields computed from the new parameterization. It is clear that the altitudinal component dominates the temperature field. The figure shows that the effect of the latitudinal component changes with time of year due to the abundance of solar radiation in summer, or lack of it in winter. The effect of the longitudinal dependence can be examined by comparing the difference maps of Figure 3a and b (including longitudinal dependence) with those of Figure 4a and b (excluding longitudinal dependence). For example, the effect can be seen in the northwestern part of Greenland, where the temperatures in Figure 3a and b show higher positive differences than in Figure 4a and b. The new temperature parameterization, in general, also yields higher temperatures over the ice sheet for the annual case, whereas the July temperature only yields higher temperatures over the north and northwestern part of the ice sheet, due to a small latitudinal dependence combined with the longitudinal component. Similar higher temperatures also exist when not taking the longitudinal component into account, but with less difference in the northwestern part of Greenland. Figure 5a and b show the difference between the new temperature parameterization with and without data from the land stations. Without the land-station data the northeastern part of Greenland appears too cold compared with observations, due to a stronger longitudinal dependence, especially in the July temperature (Table 3). This is likely to be because of the sparse station data available in the north; land stations are therefore needed to predict the temperature more accurately.

Figure 6 shows the temperature difference between the observed values from the AWS and the temperature parameterizations of this study and those of Ritz and others (1997). The differences in temperature between the parameterization of this study and the observations are also given in Table 2. Comparing the new parameterization with Ritz

https://doi.org/10.3189/002214309788608985 Published online by Cambridge University Press

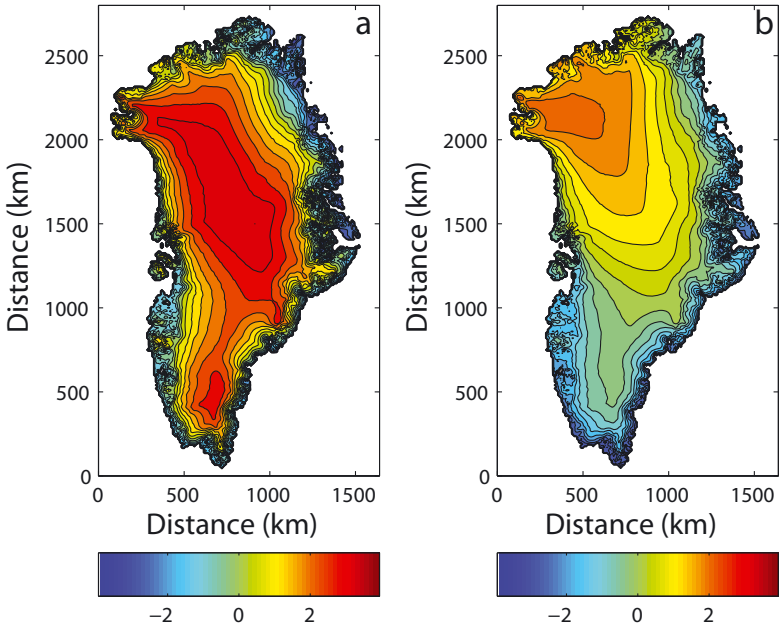

Fig. 3. The difference between the temperature parameterization for this study with a longitudinal dependence and that of Ritz and others (1997): (a) for the annual temperature and (b) for the July temperature.

and others (1997), both the annual and July temperature of the new parameterization show a better performance at 37 station sites out of 41, in relation to observations, corresponding to over 90%. The parameterizations by Ritz and others (1997) have a general overestimation at low elevations and a general underestimation at high elevations. The root-mean-square difference (rmsd) on the residuals from the temperature parameterization is given in Table 3. The values of the rmsd indicate a slight improvement when longitudinal dependence is included in the temperature parameterization.

The annual melt extent was calculated with the PDD model using both the new parameterization and the temperature parameterization by Ritz and others (1997) for a spatial resolution of 10 km. The cut-off value for the Gaussian distribution in the degree-day integral (Equation (3)) is set to 1 mm of melt, which implies that melt rates $<1\,\mathrm{mm\,a^{-1}}$ will be regarded as dry snow. The melt area extent for the parameterization by Ritz and others (1997) is $13.1 \times 10^5\,\mathrm{km^2}$ (Fig. 7b). The melt area extent from the new parameterization is $6.6 \times 10^5\,\mathrm{km^2}$ (Fig. 7a). The modelled melt area extent is

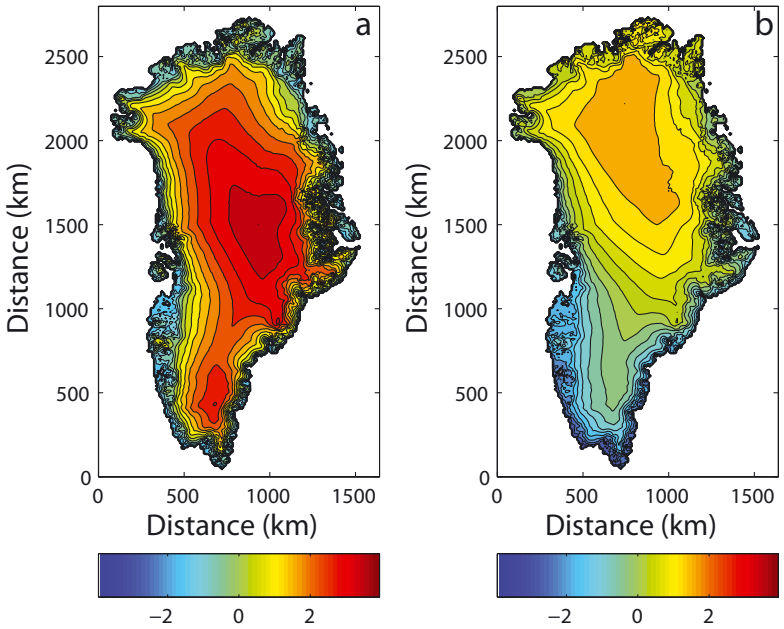

Fig. 4. Same as Figure 3 but without a longitudinal dependence.

https://doi.org/10.3189/002214309788608985 Published online by Cambridge University Press

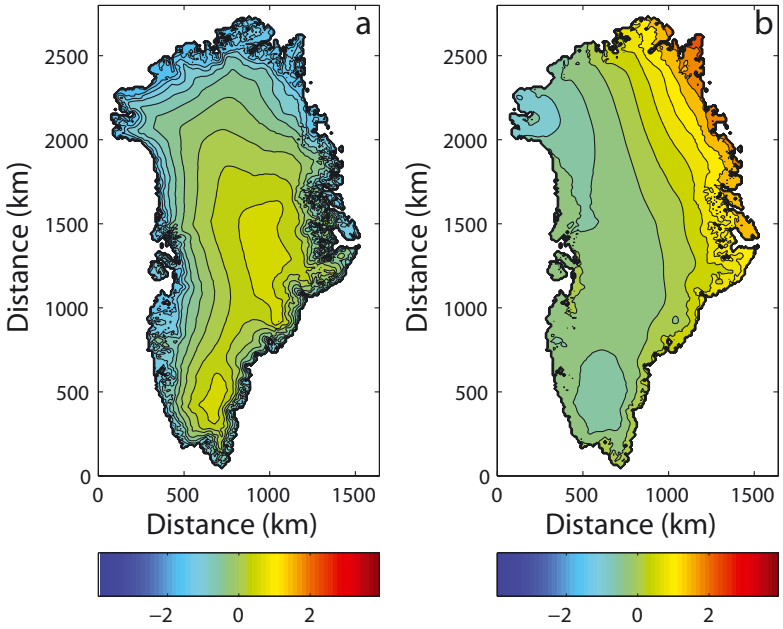

Fig. 5. The difference between the temperature parameterization for this study with and without land stations: (a) for the annual temperature and (b) for the July temperature.

then compared to a satellite-derived melt area extent. The satellite-derived melt area extent has a mean value of 4.6×10^5 km^2 calculated over a 6 year period (2000–05) based on a moderate-resolution imaging spectroradiometer (MODIS) algorithm (Fausto and others, 2007). A mean value of $\sim 4.6 \times 10^5$ km^2 for a period (1979–2002) of 24 years by Steffen and others (2004) and $\sim 5.2 \times 10^5$ km^2 for a period (1979–2005) of 27 years by Fettweis and others (2007) is calculated using passive- and active-microwave data. Wang and others (2007) derive a melt area extent using the SeaWinds scatterometer on QuikSCAT, which is an active-microwave radar (Ku-band sensor). The QuikSCAT melt area extent has a mean value of 58% for the ice-sheet area of Greenland during the period 2000–04, corresponding roughly to a melt area extent of 7.1×10^5 km^2. The largest difference in melt area extent between the modelled area and the satellite-derived area is ~18% for Fausto and others (2007), and the smallest difference is 4% for Wang and others (2007). The four satellite-derived melt area extents agree reasonably well with the PDD model using the new parameterization, which gives confidence in its applicability.

DISCUSSION

Model parameterizations of this type have been applied often to the existing ice sheets of Greenland and Antarctica, and to those which covered the continents of the Northern Hemisphere during the Quaternary ice ages (Huybrechts and

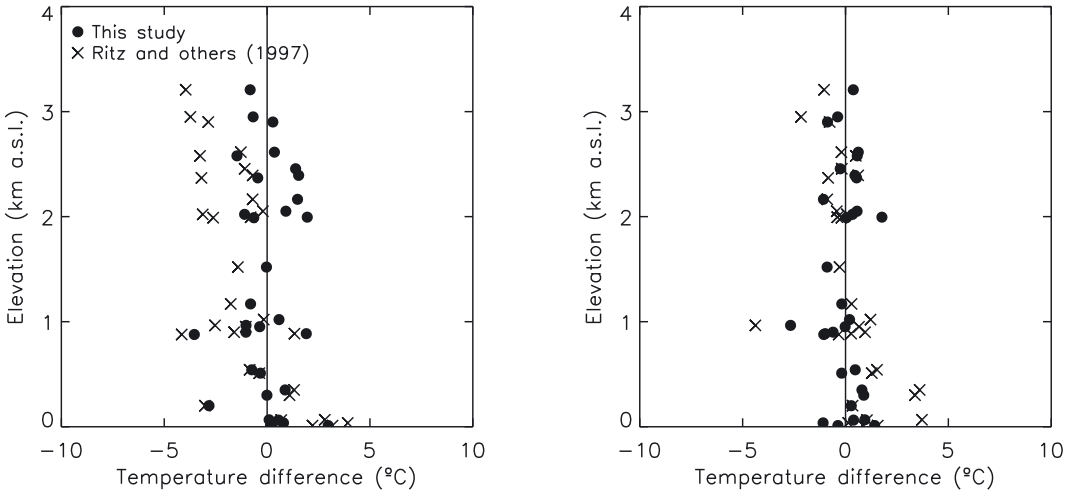

Fig. 6. The temperature difference between the observed values from the AWS and the temperature parameterizations of this study and that of Ritz and others (1997). (a) The annual temperature and (b) the July temperature.

https://doi.org/10.3189/002214309788608985 Published online by Cambridge University Press

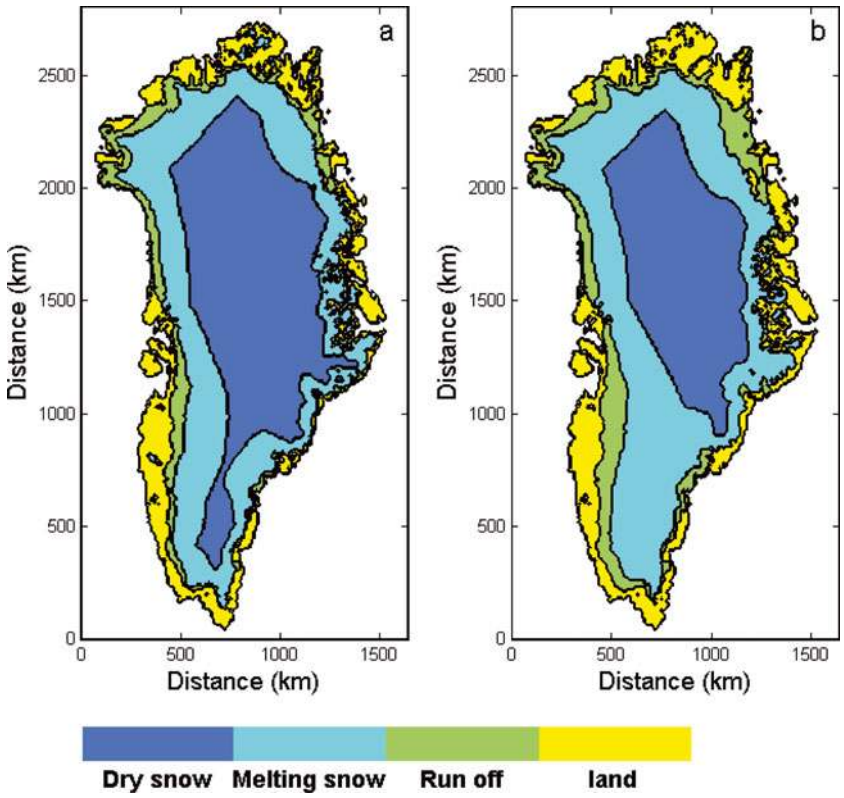

Fig. 7. (a) The annual melt area extent for this study. (b) The annual melt area extent for Ritz and others (1997).

de Wolde, 1999; Tarasov and Peltier, 1999; Greve, 2005). For example, Greve (2005) uses a glacial index, which is based on the results from ice-core data, to derive a time-dependent temperature forcing. A temperature distribution is then interpolated linearly between the present and the Last Glacial Maximum (LGM) values from a general circulation model. The glacial index scales the Greenland Icecore Project (GRIP) record to represent glacial and present conditions. The simulated anomaly from the glacial index is added to the near-surface air-temperature field over the whole region. The index is a useful tool, but it implies that the temperature distribution of Greenland can be interpolated between two climate extremes and that the climatic perturbation is the same for the whole ice sheet, which will not be the case. The parameterizations were primarily based on data from land climate stations and a few climate stations on the ice sheet. This may not give a clear picture of the evolution of the temperature field, due to different climatic and environmental conditions, and parameters that influence the temperature. However, the land-station data are needed to calculate the temperature parameterization, as without it the optimized coefficients would yield unrealistic temperatures, especially in the northeast.

The transition from land to ice further complicates the temperature distribution. Land and ice interact differently with the atmosphere. Over ice there is an ever-present shallow near-surface inversion layer, but land conditions will vary between convective and stable conditions (Grotjahn, 1993). The observed slope lapse rate could be biased by frequent inversion layers that dominate the coastal climate under conditions of low clouds or sea fog coming from the ocean (~400–500 m a.s.l.; Box and Cohen, 2006). Reeh (1991) includes a simple way to account for the coastal inversion layer in his parameterization to get a better fit to observations. It was necessary to include an inversion layer, because he used over 30 land stations and only 5 stations on the ice sheet, to parameterize his temperature field. The coastal inversion layer is not accounted for in this study because the majority of the stations used for the parameterization are located on the ice sheet. However, this could be a reason for the small discrepancy in the optimized coefficients in Equations (1) and (2) compared to the observations in Table 4.

The new temperature parameterization may not fully represent a climatological mean, as only limited data are available, obtained over different periods and sometimes for only a few months. This may therefore be responsible for a bias in the modelled temperature distribution. A proper validation of the parameterization is very difficult because all trustworthy observational data are used for optimizing the coefficients in Table 3. It could be argued that some of the station data should be used for validation. However, the scarcity of near-surface air-temperature observations and their uneven spatial and temporal distribution means that omitting any part of the dataset would cause a substantial change in the resulting optimized coefficients of Table 3.

To investigate interannual variability and the effect of varying spatial data coverage, the optimized coefficients in Equations (1) and (2) are calculated for each year in the data period (1996–2006; Table 5). The difference is quite high in some of the years when compared to the coefficients in Table 3, and the largest difference is seen in 1996 where the longitudinal dependence is negative, compared to the other years, for the July fit. However, all parameters obtained in this study (Table 3) fall within the standard deviations in Table 5. This gives us confidence that our parameters are representative of present-day conditions over the GrIS.

The modelled melt area extent agrees reasonably well with the observed fit from satellite measurements (Steffen

https://doi.org/10.3189/002214309788608985 Published online by Cambridge University Press

Table 5. Coefficients for Equations (1) and (2) and their rmsd in relation to the observed temperatures

Year	$d_{ma,j}$ °C	$\gamma_{ma,j}$ °C km^{-1}	$c_{ma,j}$ °C ° N^{-1}	$\kappa_{ma,j}$ °C ° W^{-1}	rmsd	Number of stations used
Annual fit						
1996	50.73	−4.343	−0.8178	0.0048	1.32	20
1997	46.49	−5.681	−0.7749	0.0349	1.53	25
1998	50.70	−5.439	−0.8352	0.0306	1.29	26
1999	46.79	−6.106	−0.7770	0.0427	2.07	32
2000	45.64	−6.488	−0.7671	0.0469	0.99	31
2001	45.96	−6.522	−0.7750	0.0613	1.74	33
2002	43.71	−6.428	−0.7395	0.0487	1.20	30
2003	31.40	−5.963	−0.6006	0.1269	2.61	32
2004	40.15	−6.698	−0.7005	0.0821	2.03	34
2005	33.78	−6.018	−0.6292	0.1111	2.01	33
2006	45.70	−6.109	−0.7632	0.0366	0.78	19
Mean	43.73	−5.981	−0.7436	0.0570	1.60	—
Std dev.	(±6.25)	(±0.661)	(±0.0730)	(±0.0363)	—	—
July fit						
1996	24.88	−5.777	−0.2697	−0.0087	2.34	20
1997	21.40	−6.156	−0.2406	0.0309	1.59	25
1998	14.77	−5.364	−0.1526	0.0434	1.33	26
1999	19.45	−5.402	−0.2194	0.0446	1.38	32
2000	21.48	−5.600	−0.2441	0.0321	1.42	31
2001	19.50	−5.586	−0.2185	0.0340	1.47	33
2002	12.81	−4.894	−0.1204	0.0362	1.52	30
2003	13.77	−5.894	−0.1435	0.0558	1.37	32
2004	16.43	−5.270	−0.1759	0.0380	1.32	34
2005	13.93	−4.710	−0.1433	0.0484	1.21	33
2006	16.63	−5.162	−0.1749	0.0345	1.54	19
Mean	17.73	−5.438	−0.1912	0.0354)	1.50	—
Std dev.	(±3.88)	(±0.427)	(±0.0495)	(±0.0164)	—	—

and others, 2004; Fausto and others, 2007; Fettweis and others, 2007; Wang and others, 2007). The agreement depends primarily on the degree-day factors, σ_{pdd} and the cut-off value of the Gaussian distribution in the degree-day integral. In this study, the degree-day factors were not changed compared to the work of Greve (2005) (Equations (5) and (6)), which leaves σ_{pdd} and the cut-off value to account for the variation in melt area extent produced by the PDD model. The degree-day factors in the PDD model may show considerable spatial and temporal variability, as they incorporate all the energy-balance components into a single value for very different surface and climate conditions. It is therefore important to be aware of their limitations (Ohmura, 2001; Hock, 2003).

The cut-off value of the Gaussian distribution was set to 1 mm and it can be demonstrated that the sensitivity of the calculated melt area extent to this parameter is not very large. The cut-off value of 1 mm melt rate was chosen because it is assumed that a melt rate less than a snow grain size of ~1 mm is not measurable (Bøggild and others, 1994).

It is commonly assumed that the values of σ_{pdd} span the interval 4.5–5.5°C (Reeh, 1991; Ritz and others, 1997; Tarasov and Peltier, 1999). In this study the value of $\sigma_{pdd} = 2.53$°C was chosen, based on the mean value of the standard deviations of the mean monthly temperatures from each station located on the ice sheet. This is a direct reflection of the temperature variations observed at the climate stations on the ice sheet. Lefebre and others (2002) reached a similar value for σ_{pdd} using a coupled atmosphere–ocean general circulation model for the southern part of Greenland. PDDs show a high sensitivity to changes in the value of σ_{pdd}, so it is important to constrain the value within observations. For example, it can be demonstrated that an increase of σ_{pdd} from 2.53 to 4.5°C results in an increase of 33% in the melt area extent in the model (Fig. 7). This additional source of uncertainty is often not considered in other model studies, and their corresponding standard deviation is kept fixed or used as a tuning parameter in order to get a better fit to observations (Reeh, 1991; Ritz and others, 1997; Huybrechts and de Wolde, 1999).

Using the mean value of the standard deviations of mean monthly temperatures may not necessarily be the best choice for σ_{pdd} for modelling melt on short timescales. For example, using a value of σ_{pdd} determined for different sectors on the ice sheet may be a better choice. Such an approach would require more temperature observations from stations located on the ice sheet in order to improve the spatial coverage. An even larger problem occurs on long timescales, as we cannot know the standard deviation of the mean temperatures during the ice age. Therefore, we emphasize that the σ_{pdd} value is only valid for the present. A value of $\sigma_{pdd} = 2.53$°C seems to be the best choice available for this study. The comparison between the modelled melt area extent and the satellite-derived measurements cannot qualify as a validation of the temperature parameterization because of the crude PDD method and poorly constrained degree-day factors, but the comparison tests the outcome so it can be used in large-scale ice-sheet models.

https://doi.org/10.3189/002214309788608985 Published online by Cambridge University Press

Wang and others (2007) find that the melt area extent, determined using their algorithm for enhanced-resolution QuikSCAT images, depends mostly on the variation in altitude, then on variation in latitude and least of all on the variation in longitude. This agrees with our findings. However, we have shown that longitude still plays a role in the temperature variation. The rmsd values indicate (see Results section and Table 3) that it contributes to a better agreement between model and observations. This gives an overall confidence in the inclusion of longitude in the temperature parameterization. Moreover, the spatial distribution of the AWS used in this study is, to the authors' knowledge, the most comprehensive so far.

Calculating ablation using surface energy balance (Van de Wal, 1996; Box and others, 2006) requires information about net radiation, wind speed, relative humidity and other poorly constrained variables that affect energy fluxes at the surface. Lacking input, there is no reason why energy-balance models should produce estimates of past or future ablation that are better than those based on the PDD model (Bougamont and others, 2007). To produce reliable scenarios for the GrIS, the ice-sheet models require temperature and precipitation data to reproduce the state of the ice sheet. The most reliable palaeoclimate proxies are air temperature and precipitation, which makes the PDD approach a powerful method for describing the surface mass balance in ice-sheet models.

CONCLUSION

A new temperature parameterization is used to estimate a melt area extent derived from a PDD approach. The temperature parameterization and the PDD model, which is based on physical and statistical considerations (Ohmura, 2001), allow a fast integration speed in numerical schemes. The inclusion of new observational data and a longitudinal dependence in the temperature parameterization gives more accurate sensitivity values for elevation and latitude, and has produced a reliable near-surface air-temperature map. The standard deviation of the temperature observations, σ_{pdd}, is used as direct input for the PDD model. The value of $\sigma_{\mathrm{pdd}} = 2.53^{\circ}\mathrm{C}$ is smaller than the generally used value of 4.5–5.5°C. The strength of using the new σ_{pdd} is that it mimics the observed standard deviation of the temperature measurements from the climate stations more closely. A case study using the new temperature parameterization and $\sigma_{\mathrm{pdd}} = 2.53^{\circ}\mathrm{C}$ showed that the PDD model provided a reasonable estimate for the mean melt area extent observed from satellites in Greenland. Acquisition of more temperature data and a longer time series is crucial to improve the temperature parameterization further; such an improvement closely follows the technical progress in such fields as ice-core drilling, remote sensing and the establishment of more AWS on the ice sheet. So far, the scarcity in the observational dataset precludes a proper validation of the temperature parameterization. More observational data will help improve this situation and are expected from the more than 30 AWS currently in operation on the GrIS.

ACKNOWLEDGEMENTS

We thank K. Steffen's group at the Cooperative Institute for Research in Enviornmental Sciences (CIRES) and M. van den Broeke at the Institute for Marine and Atmospheric Research Utrecht for providing temperature data from GC-Net and the K-transect, respectively. We also thank R.H. Mottram for improving the English, and J. Box, an anonymous reviewer and the Scientific Editor, R. Hock, for constructive criticism which improved the manuscript significantly. This paper is published with the permission of the Geological Survey of Denmark and Greenland.

REFERENCES

Ahlstrøm, A.P. and PROMICE project team. 2008. A new programme for monitoring the mass loss of the Greenland ice sheet. *In* Bennike, O. and A.K. Higgins, *eds. Review of survey activities 2007*. Copenhagen, Geological Survey of Denmark and Greenland (GEUS). Bulletin 15.)

Bøggild, C.E., N. Reeh and H. Oerter. 1994. Modelling ablation and mass-balance sensitivity to climate change of Storstrømmen, northeast Greenland. *Global Planet. Change*, **9**(1–2), 79–90.

Bougamont, M. *and 7 others*. 2007. Impact of model physics on estimating the surface mass balance of the Greenland ice sheet. *Geophys. Res. Lett.*, **34**(17), L17501. (10.1029/2007GL030700.)

Box, J.E. and A.E. Cohen. 2006. Upper-air temperatures around Greenland: 1964–2005. *Geophys. Res. Lett.*, **33**(12), L12706. (10.1029/2006GL025723.)

Box, J.E. *and 8 others*. 2006. Greenland ice sheet surface mass balance variability (1988–2004) from calibrated polar MM5 output. *J. Climate*, **19**(12), 2783–2800.

Braithwaite, R.J. 1995. Positive degree-day factors for ablation on the Greenland ice sheet studied by energy-balance modelling. *J. Glaciol.*, **41**(137), 153–160.

Fausto, R.S., C. Mayer and A. Ahlstrøm. 2007. Satellite-derived surface type and melt area of the Greenland ice sheet using MODIS data from 2000 to 2005. *Ann. Glaciol.*, **46**, 35–42.

Fettweis, X. 2007. Reconstruction of the 1979–2006 Greenland ice sheet surface mass balance using the regional climate model MAR. *Cryosphere*, **1**(1), 21–40.

Fettweis, X., J.P. van Ypersele, H. Gallée, F. Lefebre and W. Lefebvre. 2007. The 1979–2005 Greenland ice sheet melt extent from passive microwave data using an improved version of the melt retrieval XPGR algorithm. *Geophys. Res. Lett.*, **34**(5), L05502. (10.1029/2006GL028787.)

Greve, R. 2005. Relation of measured basal temperatures and the spatial distribution of the geothermal heat flux for the Greenland ice sheet. *Ann. Glaciol.*, **42**, 424–432.

Grotjahn, R. 1993. *Global atmospheric circulations: observations and theories.* Oxford, etc., Oxford University Press.

Hock, R. 2003. Temperature index melt modelling in mountain areas. *J. Hydrol.*, **282**(1–4), 104–115.

Huybrechts, P. and J. de Wolde. 1999. The dynamic response of the Greenland and Antarctic ice sheets to multiple-century climatic warming. *J. Climate*, **12**(8), 2169–2188.

Lefebre, F., H. Gallée, J.P. van Ypersele and P. Huybrechts. 2002. Modelling of large-scale melt parameters with a regional climate model in south Greenland during the 1991 melt season. *Ann. Glaciol.*, **35**, 391–397.

Marshall, S.J., M.J. Sharp, D.O. Burgess and F.S. Anslow. 2007. Near-surface-temperature lapse rates on the Prince of Wales Icefield, Ellesmere Island, Canada: implications for regional downscaling of temperature. *Int. J. Climatol.*, **27**(3), 385–398.

Ohmura, A. 1987. New temperature distribution maps for Greenland. *Z. Gletscherkd. Glazialgeol.*, **23**(1), 1–45.

Ohmura, A. 2001. Physical basis for the temperature-based melt-index method. *J. Appl. Meteorol.*, **40**(4), 753–761.

Paterson, W.S.B. 1994. *The physics of glaciers. Third edition.* Oxford, etc., Elsevier.

Pepin, N. and M. Losleben. 2002. Climate change in the Colorado Rocky Mountains: free air versus surface temperature trends. *Int. J. Climatol.*, **22**(3), 311–329.

https://doi.org/10.3189/002214309788608985 Published online by Cambridge University Press

Reeh, N. 1991. Parameterization of melt rate and surface temperature on the Greenland ice sheet. *Polarforschung*, **59**(3), 113–128.

Rignot, E. and P. Kanagaratnam. 2006. Changes in the velocity structure of the Greenland Ice Sheet. *Science*, **311**(5673), 986–990.

Ritz, C., A. Fabre and A. Letréguilly. 1997. Sensitivity of a Greenland ice sheet model to ice flow and ablation parameters: consequences for the evolution through the last glacial cycle. *Climate Dyn.*, **13**(1), 11–24.

Steffen, K. and J. Box. 2001. Surface climatology of the Greenland ice sheet: Greenland Climate Network 1995–1999. *J. Geophys. Res.*, **106**(D24), 33,951–33,964.

Steffen, K., J. Box and W. Abdalati. 1996. Greenland climate network: GC-net. *In CRREL Spec. Rep.* 96-27, 98–103.

Steffen, K., S. Nghiem, R. Huff and G. Neumann. 2004. The melt anomaly of 2002 on the Greenland Ice Sheet from active and passive microwave satellite observations. *Geophys. Res. Lett.*, **31**(20), L20402. (10.1029/2004GL020444.)

Tarasov, L. and W.R. Peltier. 1999. The impact of thermomechanical ice sheet coupling on a model of the 100 kyr ice-age cycle. *J. Geophys. Res.*, **104**(D8), 9517–9545.

Van de Wal, R.S.W. 1996. Mass-balance modelling of the Greenland ice sheet: a comparison of an energy-balance model and a degree-day model. *Ann. Glaciol.*, **23**, 36–45.

Van de Wal, R.S.W., W. Greuell, M.R. van den Broeke, C.H. Reijmer and J. Oerlemans. 2005. Surface mass-balance observations and automatic weather station data along a transect near Kangerlussuaq, West Greenland. *Ann. Glaciol.*, **42**, 311–316.

Wang, L., M. Sharp, B. Rivard and K. Steffen. 2007. Melt season duration and ice layer formation on the Greenland ice sheet, 2000–2004. *J. Geophys. Res.*, **112**(F4), F04013. (10.1029/2007JF000760.)

MS received 22 March 2008 and accepted in revised form 25 August 2008